Achieving high strength and high ductility of dual-phase steel via alternating lamellar microstructure

Gang Niu [a 1], Chao Ding [a 1], Zhiying Liu [b c], Xiaohang Jia [a], Haoxiu Chen [c], Na Gong [d], Yong Wang [e], Dennis TAN. Cheng Cheh [d], R.D.K. Misra [f], Huibin Wu [a]

[a] Collaborative Innovation Center of Steel Technology, University of Science and Technology Beijing, Beijing, 100083, China

[b] Max-Planck-Institut für Eisenforschung GmbH, Max-Planck-Str. 1, D-40237, Düsseldorf, Germany

[c] Department of Materials Science and Engineering, University of Toronto, Toronto, ON, M5S 3E4, Canada

[d] Institute of Materials Research and Engineering (IMRE), Agency for Science, Technology and Research (A*STAR), 2 Fusionopolis Way, Innovis #08-03, Singapore, 138634, Singapore

[e] School of Materials Science and Engineering, Nanyang Technological University, Singapore, 639798, Singapore

[f] Laboratory for Excellence in Advanced Steel Research, Department of Metallurgical, Materials and Biomedical Engineering, University of Texas at El Paso, El Paso, TX, 79968, USA

Abstract

Overcoming the strength-plasticity trade-off in GPa-grade dual-phase steel while simultaneously enhancing both properties poses a significant challenge. In this study, we propose an innovative strategy to break this inherent dilemma by designing an alternately arranged ferrite and martensite lamellar microstructure with appreciable deformation coordination in dual-phase steel. Compared to traditional dual-phase steel (DP steel) with a block microstructure and the same phase components, the newly developed heterogeneous lamellar dual-phase steel (L-DP steel) prepared by a cyclic intercritical quenching process demonstrates a remarkable 90 % increase in uniform elongation (from 9.1 ± 0.4 % in DP steel to 17.3 ± 0.3 % in L-DP steel). The ultimate tensile strength increases slightly from 1002 ± 10 MPa (DP steel) to 1034 ± 11 MPa (L-DP steel). The lamellar martensite and lamellar ferrite with a certain hardness difference lead to high back stress during plastic deformation, thereby ensuring the ultra-high

tensile strength of the L-DP steel. The improved ductility of the L-DP steel is primarily attributed to the appreciable coordinated deformation ability of the lamellar microstructure and the considerable plastic deformation ability of lamellar martensite. These two outstanding capabilities allow this unique microstructure to elongate continuously along the tensile direction, facilitating persistent work hardening without premature cracking. Furthermore, the heterogeneous hardening triggered by the mutual constraints of the lamellar microstructure during the plastic deformation also contributes additional work hardening to enhance the ductility. The design of lamellar microstructure under a cyclic intercritical quenching process presents an efficient and feasible pathway for producing GPa-grade dual-phase steel with considerable ductility.

Keywords

Dual-phase steel; Cyclic intercritical quenching process; Lamellar microstructure; Strength-ductility synergy; Plastic deformation mechanism

1. Introduction

The current industrial development focuses on energy conservation, emission reduction, and lightweight structure, which has heightened interest in high-strength structural steels and alloys [[1], [2], [3], [4], [5], [6]]. Among these steels, advanced high-strength steels with an excellent combination of strength and plasticity have gained popularity [1,7]. Despite the outstanding mechanical properties of the third-generation advanced high-strength steel, challenges related to smelting and complex heat treatment processes have hindered its widespread adoption [[8], [9], [10], [11]]. In contrast, as the first generation of advanced high-strength steel, martensitic-ferrite dual-phase steels are widely used in structural, reinforcing, and crashworthiness parts of automobiles, which thanks to remarkable attributes such as cost-effectiveness, simplified manufacturing process, and sustained yield properties throughout deformation. While the mechanical properties of this steel may not be exceptionally outstanding, it still offers acceptable performance across various applications [12,13]. Consequently, a deeper exploration of the mechanical properties of dual-phase steel is necessary to fulfill more rigorous design criteria and expand the application prospects.

The relationship between strength and ductility in metallic materials is widely recognized as a trade-off. Improving ductility without sacrificing or even increasing strength is the unifying goal of scientists across different materials fields. The attributes of dual-phase steel, excluding alloy content, are predominantly governed by the size, morphology, volume fraction, and distribution of its constituent phases [14]. The traditional dual-phase steel is composed of 20–30 vol% block martensite (providing strength) distributed within a polygonal ferrite matrix (contributing plasticity). The matching between the soft phase and hard phase is responsible for the considerable mechanical properties of dual-phase steel compared to pure ferritic or martensitic steels. Therefore, the performance of dual-phase steel can be improved by properly adjusting the ferrite and martensite structure or ratio. Grain refinement is widely employed as it simultaneously improves both strength and plasticity. For instance, Alibeyki et al. [15] obtained fine-grained dual-phase steel with a grain size of less than 5 μm through a cold rolling and annealing process, resulting in appreciable strength and ductility matching. Soleimani et al. [16] replaced traditional cold rolling with the cross-rolling process, resulting in finer grains (from 11.4 μm to 4.5 μm) and significantly improved mechanical properties after applying critical annealing. However, when the grain size is less than 1 μm, fine grain strengthening becomes evident at the expense of a serious loss of plasticity due to insufficient work hardening ability [13,17]. Therefore, further optimization of the mechanical properties of dual-phase steel can be achieved by modifying the hardness/strength difference between martensite and ferrite to improve deformation coordination. One commonly used method is tempering, which alleviates the deformation incompatibility between block martensite and ferrite by reducing the hardness/strength difference between the two phases [[18], [19], [20]]. However, the introduction of the tempering process leads to a decrease in tensile strength and the occurrence of discontinuous yield, resulting in the loss of inherent advantages in dual-phase steel [21,22]. Chandiran et al. [23,24] reported that the precipitation of an appropriate amount of nano-sized VC particles in ferrite effectively reduces the strength difference between ferrite and martensite, thereby improving both strength and uniform elongation and achieving a balanced combination of strength and plasticity. Consequently, enhancing the strength of ferrite has been recommended as a

viable technique for effectively improving the properties of martensite-ferrite dual-phase steel.

In recent years, the idea of appropriately increasing the volume fraction of martensite to reduce the alloy content in martensite to increase the plasticity of martensite has been used to improve the strength and plasticity matching of dual-phase steels [25,26]. While improving the performance of dual-phase steel by optimizing the volume fraction of martensite and grain size has gained acceptance, the existence of block microstructure limits the potential for ductility improvement [[27], [28], [29]]. Recent trends in heterogeneous materials have prompted the exploration of lamellar microstructures, which include lamellar dual-phase steel designs [[30], [31], [32]]. For instance, Gao et al. [33] fabricated lamellar dual-phase steel by warm rolling and critical annealing, which exhibited an excellent combination of strength and plasticity even with a substantial amount of martensite. Similarly, Huang et al. [34] produced a layered heterogeneous dual-phase steel through cold rolling and intercritical annealing, exhibiting enhanced work hardening ability and significantly improved mechanical properties. Additionally, Sun et al. [35] reported that the presence of lamellar microstructure in martensite provides an additional strengthening effect, which is beneficial for improving ductility. Although the mechanical properties advantages of lamellar microstructure in dual-phase steel have been widely acknowledged, most of the preparation processes for lamellar microstructure focus on severe plastic deformation combined with intercritical annealing, resulting in anisotropy of the obtained lamellar microstructures and mechanical properties [36,37]. There is a lack of systematic exploration into size refinement, distribution uniformity, and hardness distribution adjustment between lamellae.

Motivated by these considerations, we propose a novel approach involving cyclic intercritical quenching for non-equilibrium phase transformation to design a heterogeneous lamellar martensite-ferrite dual-phase steel. Multiple quenching cycles are employed to continuously divide the block microstructure, resulting in the formation of a fine and macroscopically uniformly distributed lamellar microstructure. This approach addresses challenges posed by block microstructure, resulting in a balanced interface hardness gradient in the lamellar microstructure, thereby ensuring both high strength and considerable ductility during deformation.

2. Materials and experimental processes

The investigated steels in this study possessed a nominal chemical composition of Fe-0.15C-1.77Mn-1.19Si-0.41Al-0.015Ti (in wt.%). The austenite volume fractions of the experimental steel at 810 °C and 900 °C were calculated to be 43 vol% and 93 vol%, respectively, using Thermo-calc software, as displayed in Fig. 1a. Initially, the experimental steel was melted in a vacuum-induction furnace, followed by forging into billets. Subsequently, the forged billets were subjected to a full austenitization treatment at 1200 °C for 120 min and then hot rolled into 5 mm thick sheets through multiple passes with a 30 % reduction per pass. The phase transformation curve of the experimental steel is determined using a DIL805A thermal dilatometer with a heating rate of 10 °C/s and a holding temperature of 1000 °C, as shown in Fig. 1b. The A_{c1} and A_{c3} transformation temperatures of the experimental steel were found to be 735 °C and 920 °C, respectively. The hot-rolled sheets were subjected to different cooling processes: water-quenching, resulting in the formation of lath martensite, and air-cooling, resulting in the formation of ferrite and pearlite, as illustrated in Fig. 1c1. Additionally, the air-cooled steel was heated to 810 °C at a rate of 10 °C/s and then directly quenched to room temperature, as depicted in Fig. 1c2. In contrast, the water-quenched steel was heated to 900 °C at a rate of 10 °C/s and quenched to room temperature after holding for 3 min, which was repeated three times, as indicated in Fig. 1c3. The steels subjected to intercritical quenching and cyclic quenching were marked as DP steel and L-DP steel, respectively. The microstructures and their evolutions were comprehensively analyzed using a range of advanced techniques. This involved utilizing scanning electron microscopy (SEM, Zeiss Gemini 500) equipped with electron backscatter diffraction (EBSD, Symmetry S2, Data analysis software: AZtecCrystal), nano-auger electron spectroscopy (AES, PHI-710), electron probe microanalysis (EPMA, 1720H), and transmission electron microscopy (TEM, FEI Tecnai F20). Specimens for X-ray diffraction (XRD, Bruker D8 Advance, Step: 0.1°/min, Rigaku DMAX-RB with Cu Kα radiation, Data analysis software: TOPAS 2.1) and EBSD were prepared by employing electropolishing at 18 V for 15–20 s. TEM specimens were prepared by mechanical grinding of slices to a thickness of 30–50 μm, followed by twin-jet polishing. The mechanical properties were determined by subjecting samples to uniaxial tensile tests at room temperature, employing a strain rate of approximately 1×10^{-3} s^{-1} (MTS E45.105). Dog-bone-shaped tensile samples were machined along the rolling direction from the DP and L-DP steels, with a gauge length and width of 20 mm and 5 mm, respectively. Three parallel samples were tested to confirm repeatability. The three-dimensional reconstruction of voids and cracks at the tensile fracture was performed using high-resolution micro X-ray tomography (Zeiss, Xradia 620 Versa, Data analysis software: Avizo).

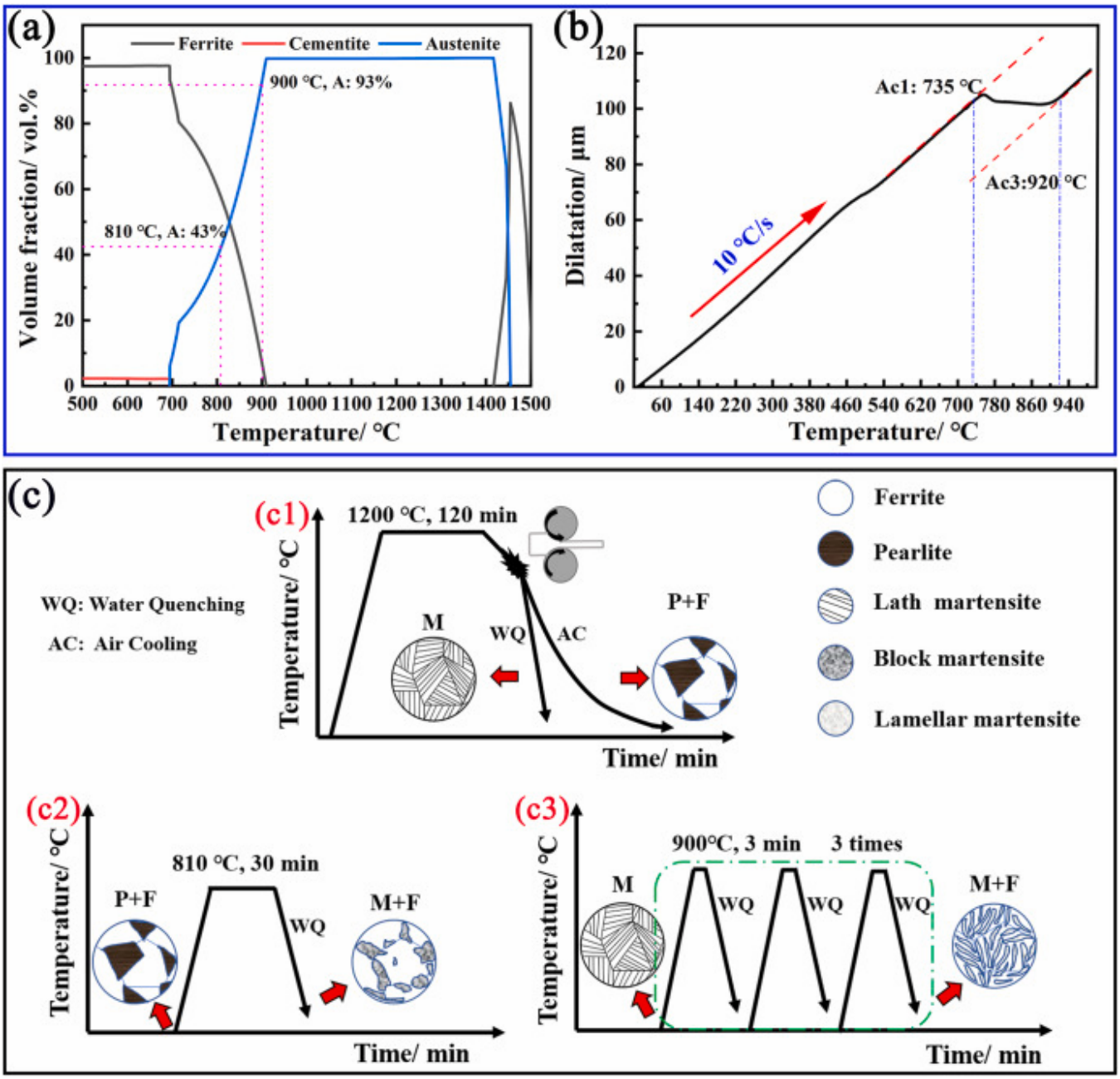

1. Download: Download high-res image (990KB)
2. Download: Download full-size image

Fig. 1. (A) The volume fraction of austenite at different temperatures is calculated by Thermo-calc software. (b) Determination of phase transformation temperatures during heating. (c) Preparation processes for the DP and L-DP steels: (c1) first water-quenching and air cooling process; (c2) preparation process for the DP steel; (c3) preparation process for the L-DP steel.

3. Results

3.1. Mechanical properties

The engineering stress-strain curves for the DP and L-DP steels are shown in Fig. 2a. The L-DP steel exhibits exceptional mechanical properties, including an ultimate tensile strength (UTS) of approximately 1034 ± 11 MPa, a uniform elongation (UE) of about 17.3 ± 0.3 %, and a total elongation (TE) of approximately 25.3 ± 0.7 %. In contrast, the DP steel demonstrates lower UTS (1002 ± 10 MPa) and reduced ductility (UE ~9.1 ± 0.4 %, TE ~16.3 ± 0.5 %). The UTS of steel L-DP is 32 MPa higher than that of the DP steel, and the UE significantly improved from ~9.1 % to ~17.3 % (an increase of 90 %). Therefore, the designed lamellar microstructure successfully enhances both UTS and ductility. Fig. 2b presents the corresponding work-hardening rate curves, indicating that both steels exhibit typical one-stage hardening behavior. Throughout the entire plastic deformation, the work-hardening rate of the L-DP steel remains higher than that of the DP steel. In the case of DP steel, the work-hardening rate rapidly decreases after the onset of yielding during plastic deformation, leading to an unstable fracture. However, the L-DP steel maintains a long-range ($0.095 \leq \varepsilon \leq 0.177$) of continuous work hardening after the DP steel instability, ensuring excellent synergy between TE (or UE) and UTS.

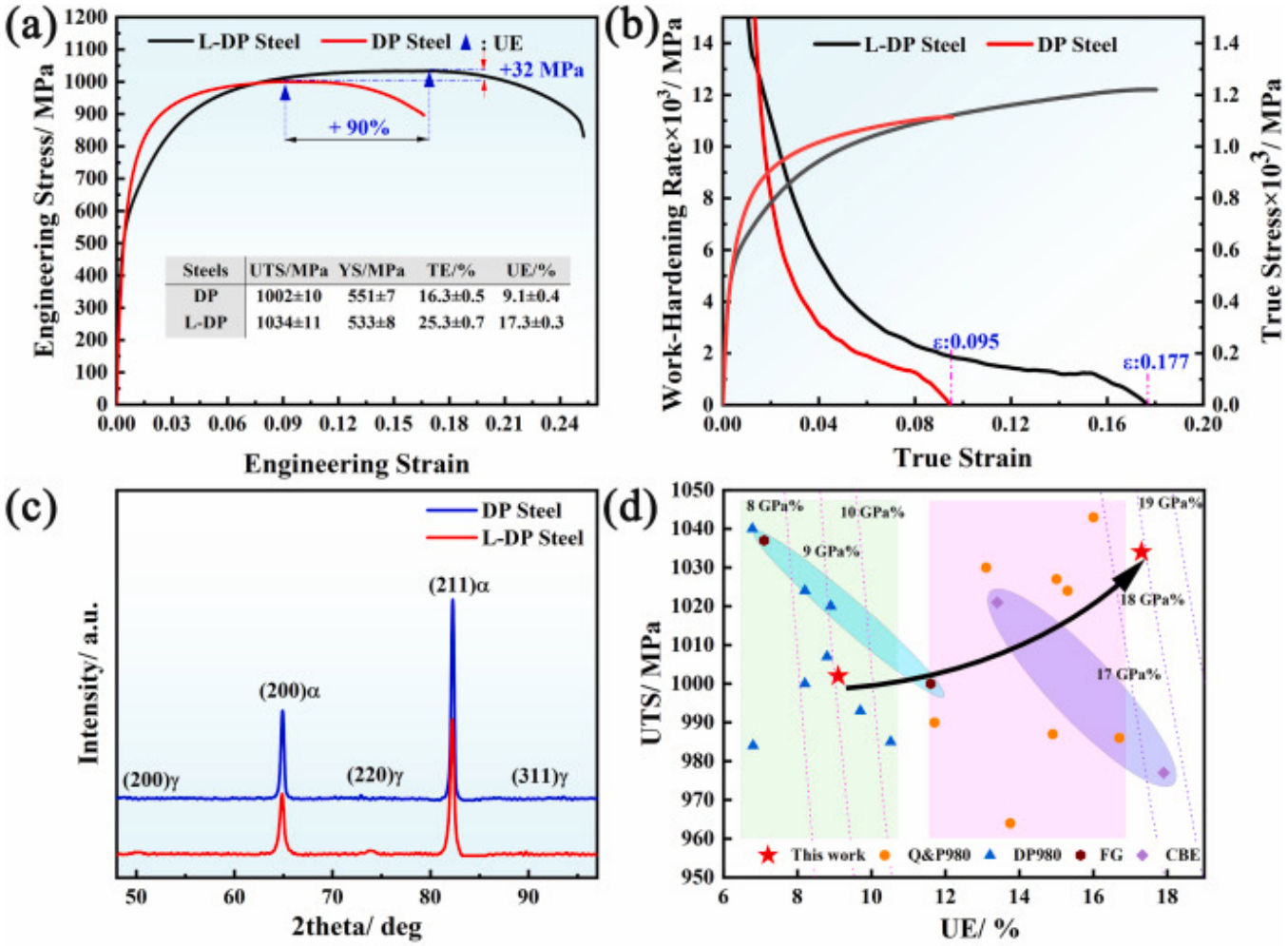

1. Download: Download high-res image (1023KB)
2. Download: Download full-size image

Fig. 2. (A) Engineering stress-strain curves. (b) Normal true stress-strain curves and work-hardening rate curves. (c) XRD diffraction pattern. (d) Statistics of mechanical properties of typical GPa grade low carbon AHSSs.

Subsequent XRD experiments are conducted to determine the volume fraction of retained austenite in the two experimental steels. Fig. 2c displays the XRD diffraction patterns of the two steels, and very weak FCC diffraction peaks are observed in L-DP steel. The volume fraction of retained austenite in L-DP steel is calculated (TOPAS 2.1 software) to be approximately 2.8 vol%. Therefore, the effect of TRIP effect on the elongation of L-DP steel is negligible in this study. The appreciable work-hardening ability of L-DP steel will be further explored in subsequent analyses. To evaluate the advantages of mechanical properties of the L-DP steel, Fig. 2d presents the mechanical performance indexes (UTS versus UE) of the L-DP steel alongside typical GPa grade AHSSs, such as Q&P980 steels [38,39], DP980 steels [40,41], FG steel [35], and chemically heterogeneous steel [42]. All steels possess a similar UTS with the range of 950 MPa–1050 MPa (GPa grade). Although the UTS and UE of the L-DP steel are not the highest, the optimal combination of UTS and UE makes L-DP steel stand out in the diagram of UTS versus UE. Additionally, the

black arrow intuitively shows that the comprehensive performance (UTS × UE, GPa·%) of the L-DP (~18 GPa·%) steel is greatly improved compared with the DP steel (~9 GP·%).

3.2. Microstructure characterization

3.2.1. SEM and EBSD analysis

To elucidate the underlying mechanisms of outstanding mechanical properties in the L-DP steel, microstructural investigations before the tensile deformation are conducted. Fig. 3a and d presents the SEM maps of DP and L-DP steels, respectively. The DP steel exhibits a conventional duplex microstructure characterized by polygonal ferrite and block martensite distributed along the primary austenite grain boundaries. In contrast, the L-DP steel depicts a special microstructure with lamellar martensite and lamellar ferrite arranged alternately, which exhibit heterogeneity at the micro level and is randomly and uniformly distributed at the macro level. The band contrast (BC) combined grain boundary (GB) maps and phase distribution maps of the two steels are shown in Fig. 3b and d, and Fig. 3e and f, respectively. In the BC map, the contrast in ferrite regions of DP steel is notably low (bright and white), while it is high in the martensite areas (black). In contrast, the contrast difference between the lamellar structures in the L-DP steel is low and overall appears gray. The higher the contrast difference in the BC map, the greater the distortion difference in the microstructure [43]. Further analysis employing machine learning phase classification in the AztecCrystal software reveals that the volume fraction of martensite (M) and ferrite (F) are 43.6 % and 56.4 % for the DP steel and 44.3 % and 55.7 % for the L-DP steel, respectively. The volume fractions of martensite and ferrite in the two steels are almost the same, which also validates the original intention of the experimental design. At an equilibrium temperature of 810 °C, the calculation result of Thermo-calc shows that the volume of austenite is 43 % (Fig. 1a), which is highly consistent with the experimental results of martensite volume fraction (43.6 %) in DP steel. Theoretically, a 93 % volume fraction of austenite should be obtained at an equilibrium temperature of 900 °C, while the volume fraction of martensite in L-DP steel is only 44.3 %, indicating that the actual volume fraction of austenite is significantly lower than the equilibrium value. In conjunction with Fig. 2c, the influence of retained austenite is eliminated. Therefore, the above analysis results imply that the incomplete formation of austenite and the continuous segmentation of the block structure through multiple cycles contribute to this phenomenon. The details of microstructure evolution during cyclic intercritical quenching are shown in Figs. S1, S2, and S3.

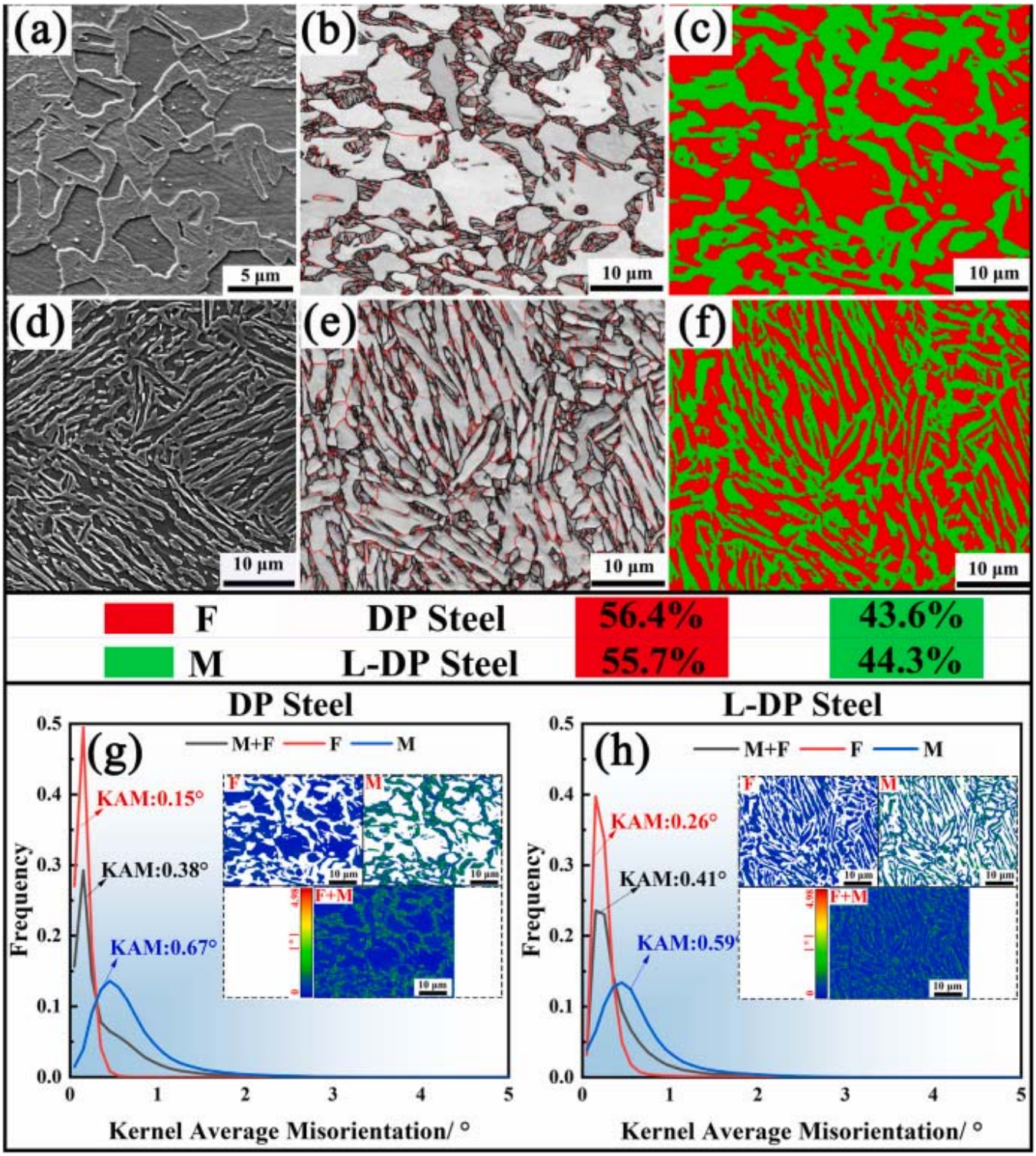

1. Download: Download high-res image (3MB)
2. Download: Download full-size image

Fig. 3. Microstructure characterization. SEM maps of DP (a) and L-DP (d) steels. BC + GB maps of DP (b) and L-DP (e) steels. The volume fraction statistical maps of martensite

(M) and ferrite (F) in the DP (c) and L-DP (f) steels. KAM distribution and statistics of F + M, M, and F of DP (g) and L-DP (h) steels.

The KAM (Kernel Average Misorientation) maps of the DP and L-DP steels, along with the corresponding martensite and ferrite phases, are shown in Fig. 3g and h. A comparison of the KAM distribution maps reveals that martensite has a higher KAM than ferrite. Additionally, the KAM distribution statistics align with the trends observed in the BC maps. Specifically, the L-DP steel displays a higher KAM for ferrite and a lower KAM for martensite compared to the DP steel. This is reflected in the KAM values of ferrite + martensite, ferrite, and martensite in the L-DP steel (DP steel), measuring 0.41° (0.38°), 0.26° (0.15°), and 0.59° (0.67°), respectively. This demonstrates that the L-DP steel exhibits a higher distortion or dislocation density for ferrite and a lower distortion or dislocation density for martensite compared to the DP steel [44]. Therefore, the difference or gradient in distortion or dislocation density between the two phases in L-DP steel is less than in DP steel. This results in a smaller hardness difference or gradient between martensite (6.3 ± 0.5 GPa) and ferrite (4.2 ± 0.3 GPa) in L-DP steel than in DP steel (7.7 ± 0.6 GPa for martensite and 3.0 ± 0.6 GPa for ferrite) measured by the nanoindentation method (Fig. S4).

Fig. 4a–c and 4d-4f show the inverse pole figure (IPF) diagrams of the DP and L-DP steels, respectively. In the DP steel, each massive ferrite displays a single orientation, while the martensite along the primary austenite grain boundary shows diverse orientations. This phenomenon indicates that during the austenitizing process of the DP steel, austenite mainly nucleates at the pearlite position with complex orientation, leading to the formation of austenite with different orientations and ultimately forming block martensite with varying orientations during the quenching process. In contrast, the orientation of the L-DP steel exhibits clear lamellar characteristics, with multiple orientations within a single original austenite grain. The orientation of each lamellar ferrite or martensite in the L-DP steel is consistent, differentiating it from the DP steel. The primary austenite grain boundaries and the martensite lath boundaries are the main nucleation sites during the austenitizing nucleation process of L-DP steel (Fig. S3), and due to the existence of the martensite packets, the lamellar microstructure orientation forms an alternating arrangement [45,46]. This consistency in orientation further validates the formation process of the lamellar microstructure (Figs. S1–S3). The grain boundary distribution statistics for the DP and L-DP steels are shown in Fig. 4g and h, respectively. Low-angle grain boundaries (LAGBs, 2–15°), medium-angle grain boundaries (MAGBs, 10–15°), and high-angle grain boundaries (HAGBs, >15°) are marked with red, green, and black, respectively. LAGBs are distributed in martensite, while MAGBs and HAGBs are located near the phase boundary in both steels. Furthermore, both steels display a similar percentage of HAGBs, with DP steel at 63.5 % and L-DP steel at 62.3 %.

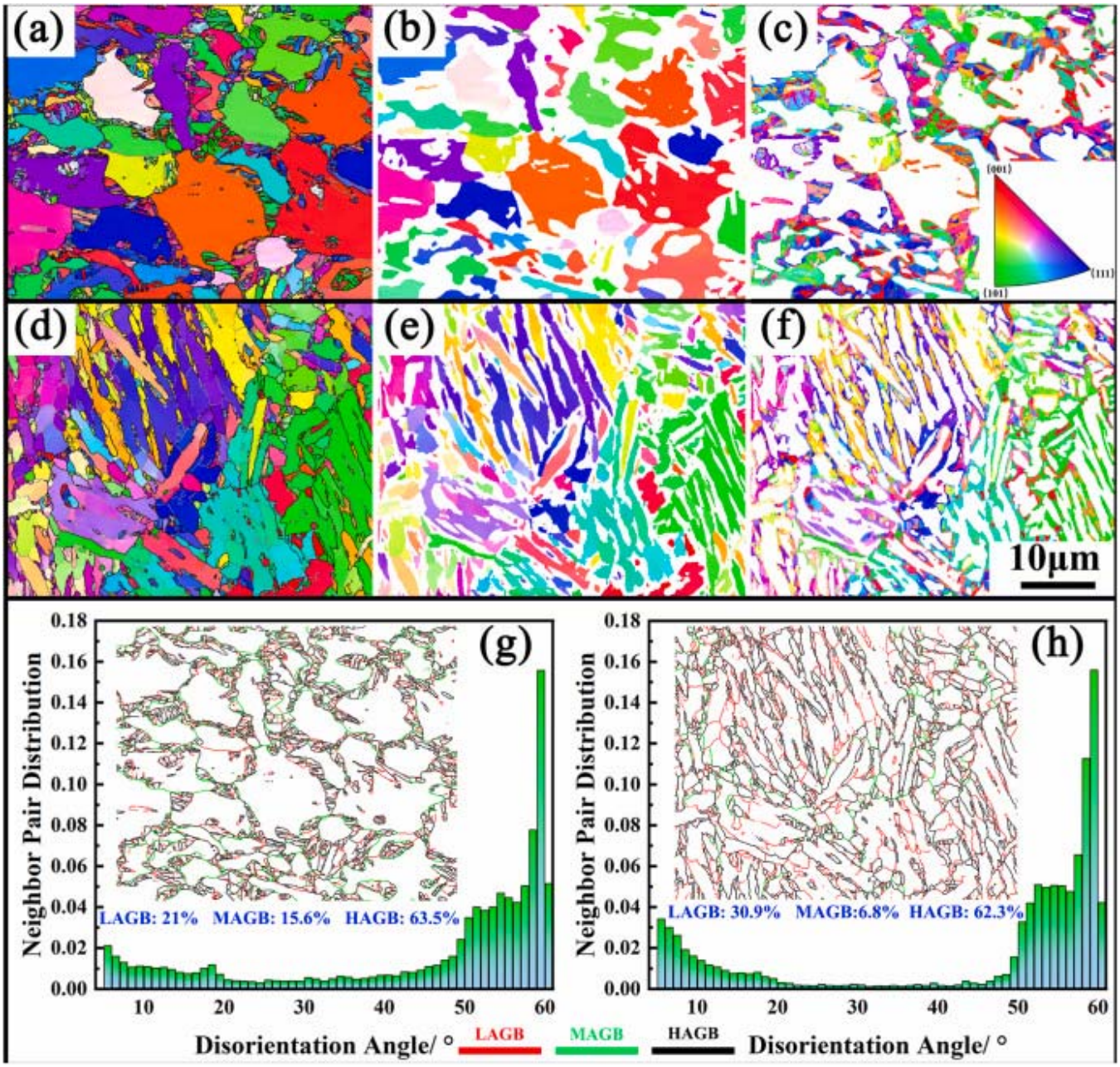

1. Download: Download high-res image (4MB)
2. Download: Download full-size image

Fig. 4. IPF maps of ferrite + martensite (a), ferrite (b), and martensite (c) of DP steel. IPF maps of ferrite + martensite (d), ferrite (e), and martensite (f) of L-DP steel. Grain boundary distribution of DP (g) and L-DP (h) steels.

3.2.2. Characterization of elements distribution

The distribution of Mn in the DP and L-DP steels is determined through Electron Probe Microanalysis (EPMA). Combining Fig. 5a and c, it can be observed that Mn is mainly enriched in martensite in both steels, while ferrite is the region with low Mn content.

Furthermore, although the volume fraction of martensite/ferrite in the two steels is the same, the proportions of Mn in these two phases are different. The difference in Mn content between martensite and ferrite is more pronounced in the DP steel compared to the L-DP steel. The decrease of alloy element concentration gradient difference may also be one of the reasons for the decrease of strain difference between the soft phase and hard phase. The decrease in the concentration difference or gradient of alloying elements in the L-DP steels also contributes to the decrease in the hardness difference between the soft and hard phases.

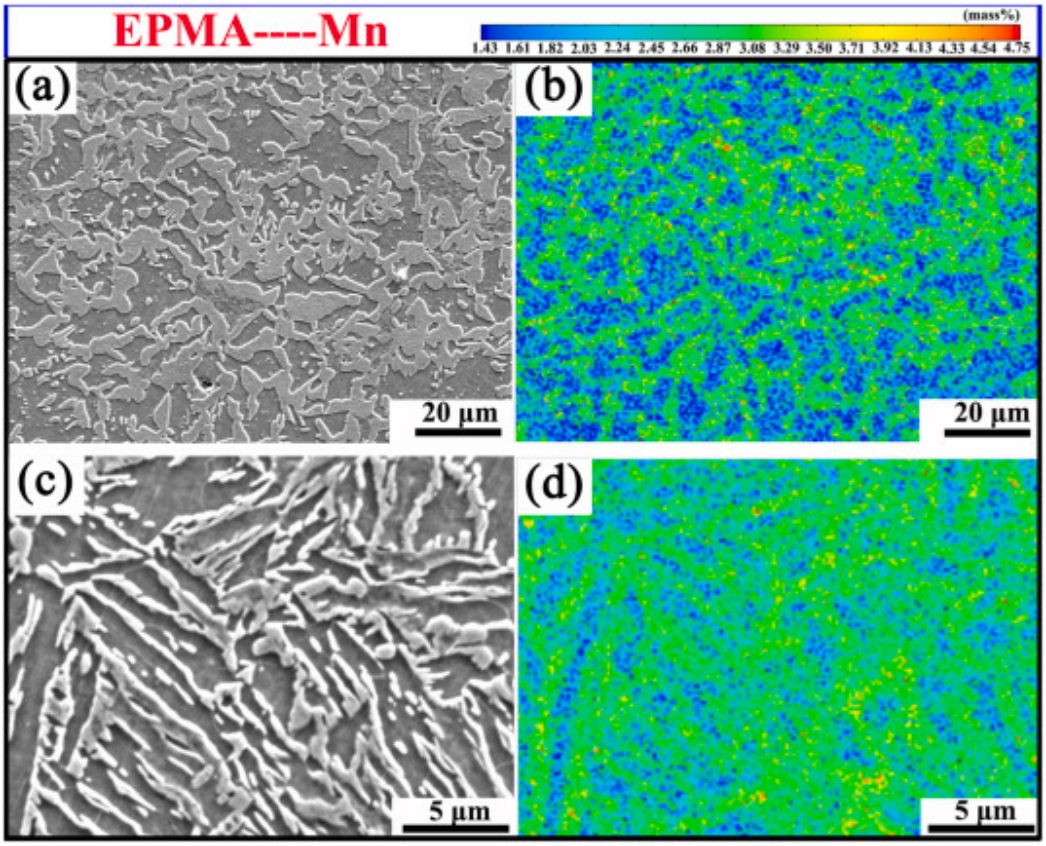

1. Download: Download high-res image (2MB)
2. Download: Download full-size image

Fig. 5. The distribution of Mn in DP steel (a, b) and L-DP steel (c, d).

To further analyze the distribution of alloying elements in the DP and L-DP steels, a nano-AES line scan is conducted to determine the mass percentage of C and Mn in martensite and ferrite [47], as shown in Fig. 6. In agreement with the EPMA results, Mn is predominantly enriched in martensite. The mass percentage of Mn in lamellar martensite fluctuates between 2.0 wt% and 2.5 wt%, and the mass percentage of Mn in lamellar ferrite is between 1.3 wt% and 1.5 wt% in the L-DP steel. For the DP steel, typical block martensite is selected for elemental analysis, revealing that the Mn content in martensite ranges from 2.5 wt% to 3 wt%, while in ferrite it is between 1.1 wt% and 1.3 wt%. In comparison, the Mn content in the L-DP steel is lower in martensite and higher in ferrite, indicating a smaller concentration difference of Mn between these two phases than that of the DP steel. The enrichment trend of C in the two phases of the DP and L-DP steels is

similar to that of Mn. However, the difference is that the concentration difference of C in the two phases of the two steels is similar. Additionally, Si and Al, as ferrite-forming elements, exhibit significantly higher concentrations in ferrite compared to martensite in both DP and L-DP steels. However, the concentration difference of Si and Al in the two phases of the two steels is also comparable. Therefore, the distribution features of Mn have an important influence on the microstructure and properties of the two steels in this study. The equilibrium uniaxial phase diagram calculated by Thermo-calc software obtained the mass percentage of elements in austenite and ferrite during holding at 810 °C and 900 °C (Fig. S4). According to theoretical calculations, when the phase transformation reaches equilibrium, the mass percentage of Mn in austenite and ferrite for DP steel (L-DP steel) is 2.54 % (1.83 %) and 1.2 % (1.3 %), respectively. This indicates that the detection results of Mn concentration in the two phases of DP steels are consistent with the calculated results. It also further implies that the L-DP steel is obtained by non-equilibrium phase transformation.

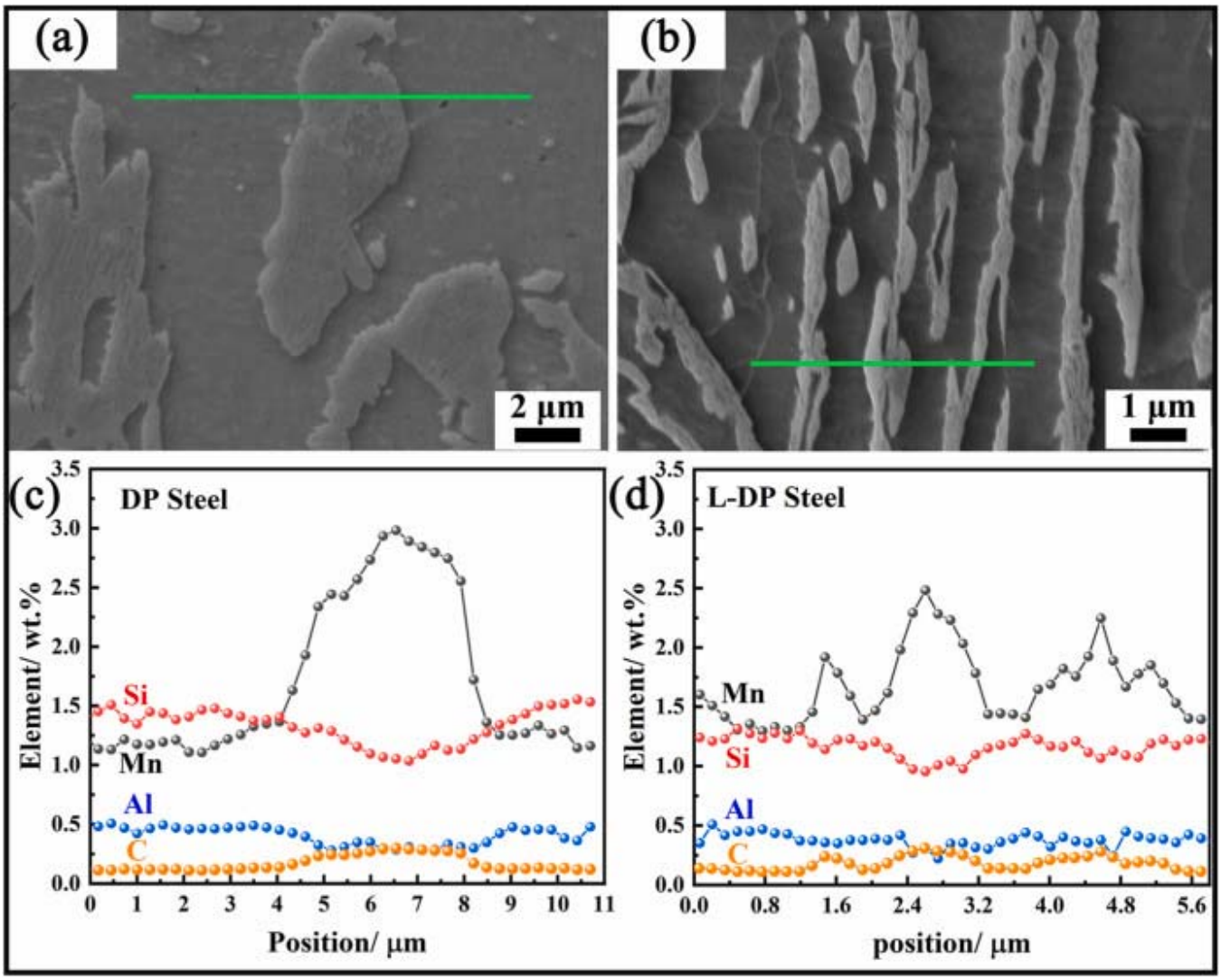

1. Download: Download high-res image (952KB)
2. Download: Download full-size image

Fig. 6. Analysis of different alloying elements in DP steel (a, b) and L-DP steel (c, d) by nano-Auger line scan.

3.3. Fracture microstructure observation

To elucidate the difference in plastic deformation characteristics between DP and L-DP steels, we conduct a comprehensive analysis of voids distribution, quantity, and size near the tensile fracture, as illustrated in Fig. 7. A total of 10 images are selected for voids quantification on the fracture surface using IPP (Image Pro Plus) software. Fig. 7a reveals that the DP steel exhibits a densely populated void distribution with varying sizes, characterized by chaotic void expansion directions. Statistical analysis of these images indicates that the voids of 0–100 pixels in DP steel exceed 1000/mm^2. In contrast, Fig. 7b demonstrates that the L-DP steel possesses a more regular void distribution pattern along the tensile loading direction, and the number of voids within the 0 to 100 pixels range does not exceed 500/mm^2. Furthermore, the maximum void area in the L-DP steel does not surpass 240 pixels^2, significantly smaller than the corresponding 500 pixels^2 observed in the DP steel. To further characterize the defects at the fracture, X-ray tomography is used to reconstruct the three-dimensional morphology of the defects (Fig. 7c–d). It can be observed that in addition to a large number of voids, there are also large-sized cracks (50–200 μm) in DP steel. Moreover, the number and size of cracks and voids in the DP steel are significantly higher than those in L-DP steel. Based on equivalent diameter statistics and three-dimensional morphology analysis, the volume fraction and average diameter of voids in the DP steel (L-DP steel) are 10.6 % (3.1 %) and 5.3 μm (3.5 μm), respectively.

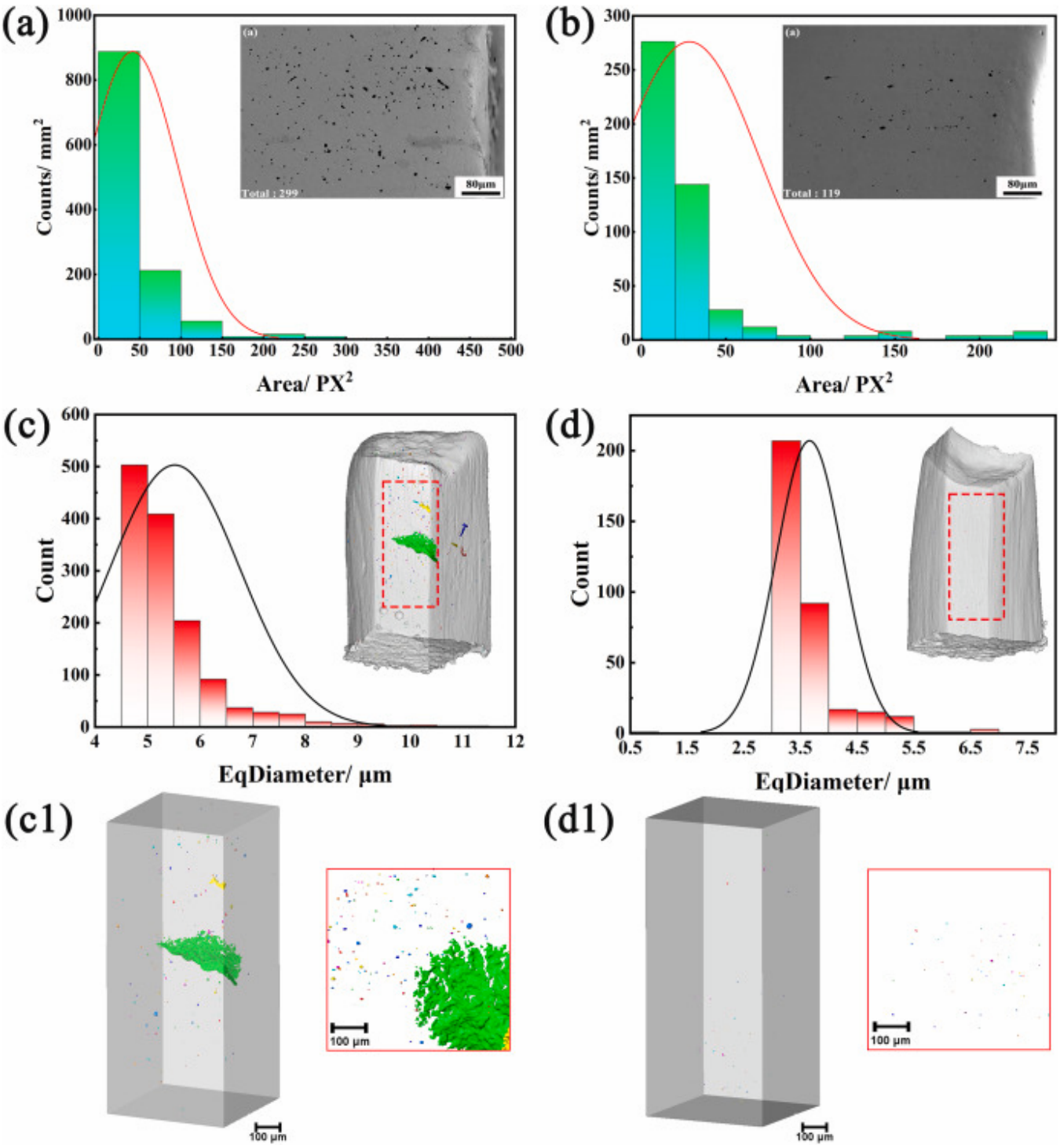

1. Download: Download high-res image (1MB)
2. Download: Download full-size image

Fig. 7. Distribution statistics of voids at the fracture of DP steel (a, c, and d) and L-DP steel (b, d, and e)

(a, b) SEM observation and statistics of two steels. (c, d) Three-dimensional reconstruction of two steel voids by high-resolution micro X-ray tomography. (c1, d1)

Magnifications of the red dashed boxes and corresponding top views of the marked area in c and d, respectively. (For interpretation of the references to colour in this figure legend, the reader is referred to the Web version of this article.)

Further microstructure observations near the fracture of the DP and L-DP steels are conducted using backscattering and secondary electron modes in SEM, as shown in Fig. 8a and b, respectively. In the DP steel, voids appear at the ferrite/martensite interface along the tensile direction. The block ferrite undergoes severe plastic deformation under high stress, while the block martensite exhibits obvious cracks, but no evident plastic deformation characteristics are observed, as shown in Fig. 8a. In the L-DP steel, both martensite and ferrite undergo plastic deformation, with martensite demonstrating a phenomenon similar to necking in areas of severe plastic deformation, as illustrated in Fig. 8b. Fig. 8c shows ferrite cracking, martensitic cracking, and phase interface cracking after severe plastic deformation at the fracture in the DP steel. It can be observed that even in the crack area with severe deformation, martensite still does not exhibit significant plastic deformation characteristics. Fig. 8d shows that lamellar martensite and lamellar ferrite always undergo intense plastic deformation together, and intense stretching of the lamellar martensite as well as post-stretching plastic fracture are observed without significant phase interface cracking. This indicates that lamellar martensite also possesses considerable plastic deformation capacity.

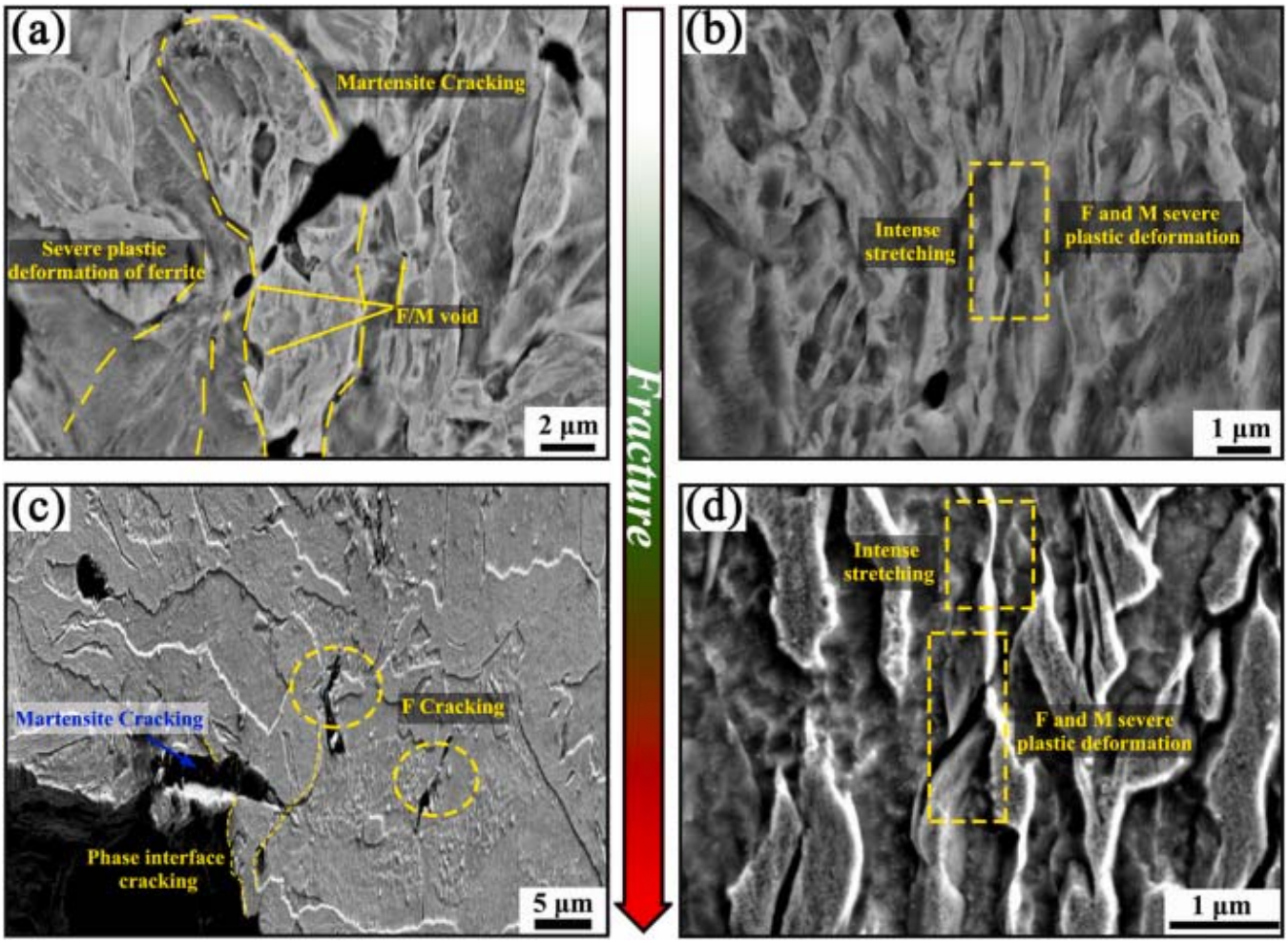

1. Download: Download high-res image (1MB)
2. Download: Download full-size image

Fig. 8. Microstructure observation near the fracture of DP steel (a, c) and L-DP steel (b, d).

4. Discussion

4.1. Distribution analysis of Mn between ferrite and martensite

A novel cyclic intercritical quenching process characterized by incomplete austenitizing has been developed to achieve fine and lamellar dual-phase steel. This cyclic treatment process significantly affects the distribution of elements in dual-phase steel and thus affects its mechanical properties. Finally, after the cyclic non-equilibrium diffusion treatment, the Mn element in ferrite is higher than the theoretical content, while the Mn element in martensite is lower than the theoretical content. Fig. 9 illustrates the formation process of Mn element distribution in the microstructure at room temperature by combining the phase transformation during heat treatment of two experimental steels. In the case of the DP steel, the initial microstructure at room temperature consists of Mn-rich pearlite and Mn-poor ferrite, as shown in Fig. 9a. As the temperature rises to the set parameter of 810 °C, the Mn element segregates towards the nucleation sites of austenite in preparation for nucleation of austenite. As demonstrated in Fig. 9b, the initial nucleation of austenite predominantly occurs within the pearlite phase. Subsequently, Fig. 9c illustrates that with an increase in holding time, the phase transformation reaches equilibrium, resulting in the formation of approximately 43 vol% austenite at this temperature (Fig. 1a). The mass percentage of Mn in austenite is calculated to be 2.54 wt% (Fig. S5a), while ferrite retains Mn content of 1.2 wt% (Fig. S5b). Considering negligible retained austenite proportions after quenching at this temperature, it can be considered that the Mn content in martensite and ferrite at room temperature remains unchanged, as displayed in Fig. 9d.

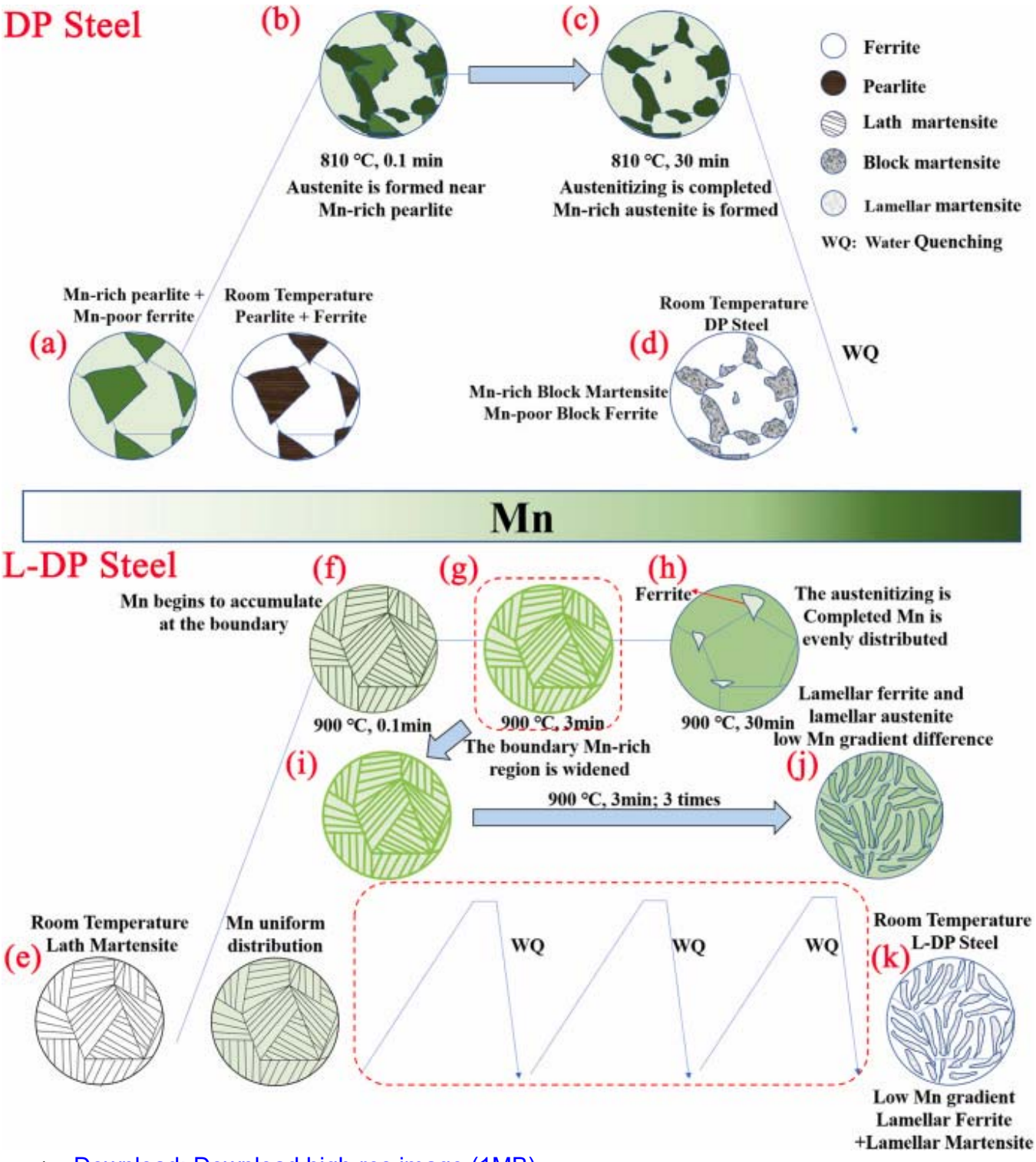

1. Download: Download high-res image (1MB)
2. Download: Download full-size image

Fig. 9. The formation process of Mn element distribution in the DP (a–d) and L-DP (e–k) steels by combining the phase transformation during the two heat treatment processes.

The initial microstructure of the L-DP steel is lath martensite, characterized by a relatively uniform element distribution, as shown in Fig. 9e. As the temperature increases, austenite nucleates on the boundaries of martensite lath, and the Mn element accumulates at these boundaries [39,46,48], as shown in Fig. 9f. After holding for 3 min, a small amount of lamellar reverse austenite forms along the boundaries of the martensite lath [49], as shown in Fig. 9g. Subsequently, with sufficient holding time, the phase transformation is completed, resulting in the formation of approximately 93 % austenite and the appearance of small polygonal ferrite, as shown in Fig. 9h. At this stage, due to the substantial presence of austenite, the Mn content in austenite (ferrite) reaches 1.83 % (1.07 %) (Figs. S4a and S4b). Fig. 9i shows the process of non-equilibrium phase transformation, and the heat treatment process is repeated three times. Finally, this process results in an element distribution effect as shown in Fig. 9j, with Mn content in austenite (ferrite) at approximately 2 wt% (1.3 wt%). The concentration difference between the hard and soft phases (ΔMn) is reduced from 1.4 % to 0.7 %. Similarly, the element content of martensite and ferrite, quenched to room temperature, remains consistent with that of high-temperature austenite and ferrite, respectively. Therefore, the new heat treatment process of non-equilibrium phase transformation not only achieves a fine and alternately arranged lamellar microstructure but also reduces the difference in element concentration between the martensite and ferrite. The L-DP steel, compared with the DP steel, effectively reduces the Mn content in martensite and increases it in ferrite while maintaining the same ratio of martensite to ferrite. This improvement in element distribution reduces the difference in solid solution strengthening of alloy elements between the two phases, which is beneficial for improving the strain matching of the two phases during plastic deformation and ultimately enhancing their coordinated deformation ability [50,51].

4.2. Relationship between microstructures and mechanical properties

Although the volume fractions of martensite and ferrite in DP steel and L-DP steel are the same, L-DP steel exhibits better mechanical properties. To comprehend the distinctions in mechanical properties between these two steels, the fracture microstructure morphology, and heterogeneous hardening are systematically examined. TEM images provide a more detailed microstructure analysis, as shown in Fig. 10. The DP steel displays an evident block structure, similar to the SEM image, whereas the L-DP steel exhibits a lamellar structure, as shown in Fig. 10a and b, respectively. Notably, in the DP steel, the polygonal ferrite with a few defects is surrounded by high-density dislocation martensite. In contrast, the dislocation density of lamellar martensite in the L-DP steel is lower, while the dislocation density of lamellar ferrite is higher. This observation is congruent with the KAM map (Fig. 3g and h), demonstrating that the difference in distortion or hardness between martensite and ferrite in the L-DP steel is lower than that in the DP steel [52,53]. An appropriate reduction in hardness disparity can effectively enhance the deformation compatibility of dual-phase steel [54].

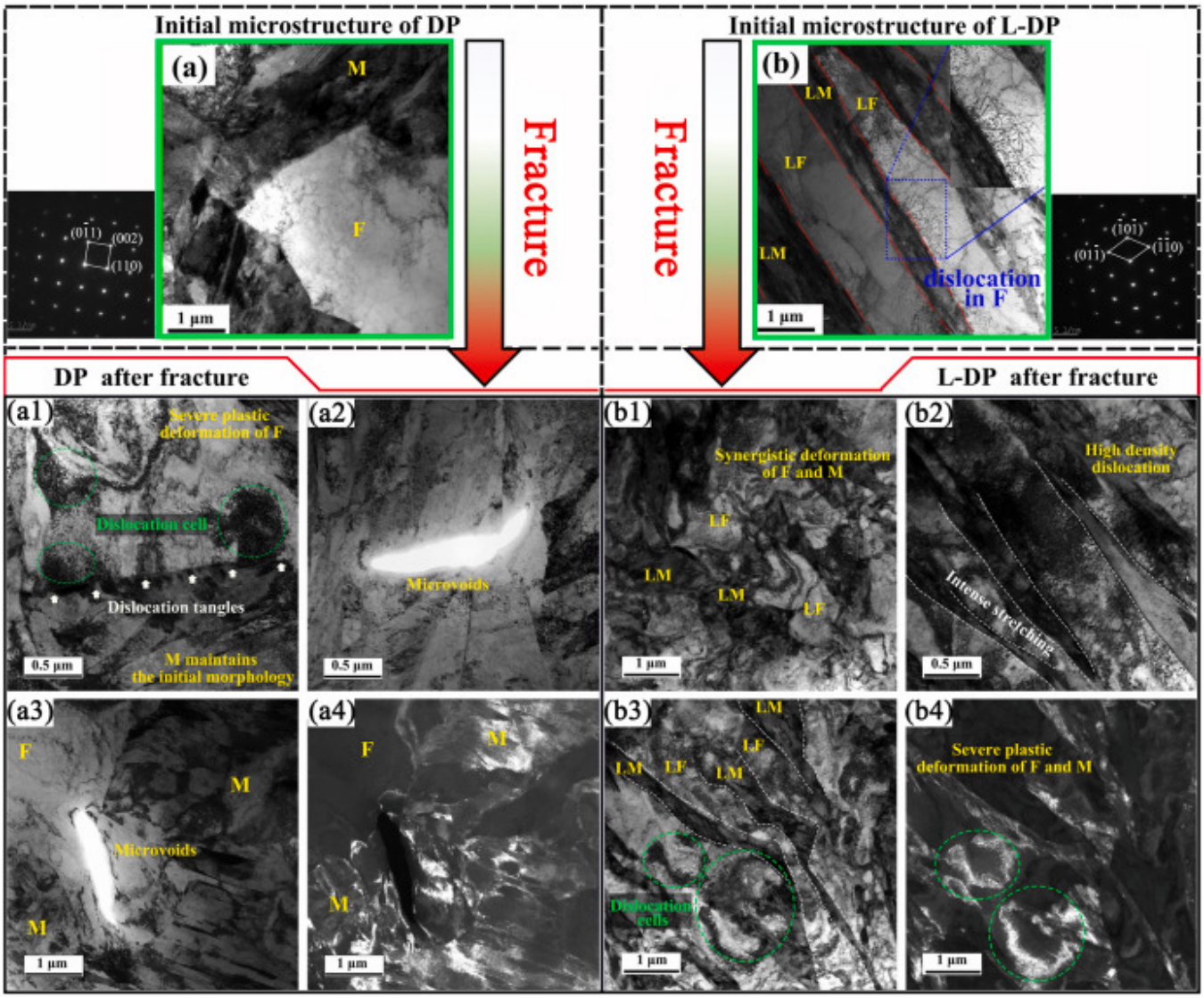

1. Download: Download high-res image (2MB)
2. Download: Download full-size image

Fig. 10. Fig. 10. TEM micrographs of the DP steel (a-a4) and L-DP steel (b-b4) before (a, b) and after (a1-a4, b1-b4) fracture. The lower left of (a) and the lower right of (b) are selected-area diffraction patterns of block martensite and lamellar martensite, respectively. TEM bright field image and corresponding dark field image in the DP (a3, a4) and L-DP (b3, b4) steels. LM and LF indicate lamellar martensite and lamellar ferrite, respectively.

The fracture microstructure of the DP steel is further detailed in Fig. 10a1-a4. Fig. 10a1 illustrates polygonal ferrite and block martensite after severe deformation. Large polygonal ferrite exhibits non-uniform plastic deformation and local stress concentration, resulting in severe dislocation tangles at the martensite-ferrite interface (indicated by white arrows). Additionally, dislocation cells can also be observed in some areas of the ferrite (green circle). The block martensite, however, exhibits no notable plastic deformation ability. This deformation mode is a typical feature of plastic deformation in

block-structured dual-phase steel [55,56]. Specifically, as tensile strain increases, polygonal ferrite undergoes plastic deformation first. Due to the significant disparity in deformation capabilities between martensitic and ferrite, rapid stress concentration occurs at the two-phase interfaces and high-density dislocation tangles occur in the ferrite. Block martensite exhibits virtually no plastic deformation capability, rendering it incapable of sustaining constraints on ferrite. Therefore, the work hardening rate decreases rapidly at this stage (Fig. 2b). Such uneven strain deformation obstructs stress transfer and facilitates the premature generation of microvoids within the phases, phase interfacial debonding, and brittle martensite cracking (Fig. 10a2). Bright and dark field images in Fig. 10a3 and 10a4 depict voids at the martensite-ferrite interface. Voids appear at the martensite interface, providing a means to release severe stress concentration resulting from the difficulty of plastic deformation in block martensite. This can be demonstrated by the disappearance of high-density dislocations and reduced bright field contrast at void edges in Fig. 10a3. Furthermore, the cracking of one martensite region does not release stress in adjacent martensite regions, perpetuating high-stress concentration and contributing to rapid block structure failure following crack initiation. The high strength and excellent ductility of the L-DP steel during deformation can be attributed to the considerable plastic deformation ability of martensite and the alternating distribution of the lamellar structure. Specifically, In the initial stage of deformation, the lamellar ferrite undergoes uniform deformation, while the high initial dislocation density (Fig. 10b) compensates for the slightly lower strength of lamellar martensite (compared to the block martensite). This ensures that the overall yield strength is not significantly reduced. The excellent plastic deformation ability of lamellar martensite and the reduced hardness difference between the soft phase and the hard phase make the L-DP steel continue to deform stably after yield. Fig. 10b1 illustrates the relatively uniform distribution of high-density dislocations in the lamellar structures, reflecting synergistic deformation between martensite and ferrite. Fig. 10b2 highlights the elongation and thinning of the lamellar structures due to severe deformation, with no apparent void characteristics. Besides, bright and dark field images in Fig. 10b3 and 10b4 demonstrate that the contrast difference between alternating lamellar structures is relatively small, exhibiting bending or even necking-like characteristics, suggesting an appreciable deformation synergy between refined martensite and ferrite under high strain. Therefore, the considerable plastic deformation ability of martensite and the appropriate hardness difference between the lamellar martensite and lamellar ferrite make the L-DP steel continue to deform stably after yield.

In addition, the excellent strength and ductility synergy of the L-DP steel is attributed to the hetero-deformation induced (HDI) hardening of the lamellar microstructure [57,58], which can be evaluated through LUR (load-unload-reload) tensile tests at various strains [59]. Fig. 11a displays the typical LUR true stress-strain hysteresis loop (solid line) and the initial uniaxial tensile true stress-strain curve (dotted line). HDI stresses are calculated using the following equation [59]:

$$\sigma_{\mathrm{HDI}} = (\sigma_r + \sigma_u)/2 \quad (1)$$

where σ_{HDI}, σ_r, and σ_u represent back stress, reloading yield stress, and unloading yield stress, respectively. The yield point is determined based on a 5 % deviation of stress-strain slope ($\Delta\sigma true/\Delta\varepsilon true$) from the effective Young's modulus [30]. The calculated back stresses of the DP and L-DP steels under different true strains are shown in Fig. 11b.

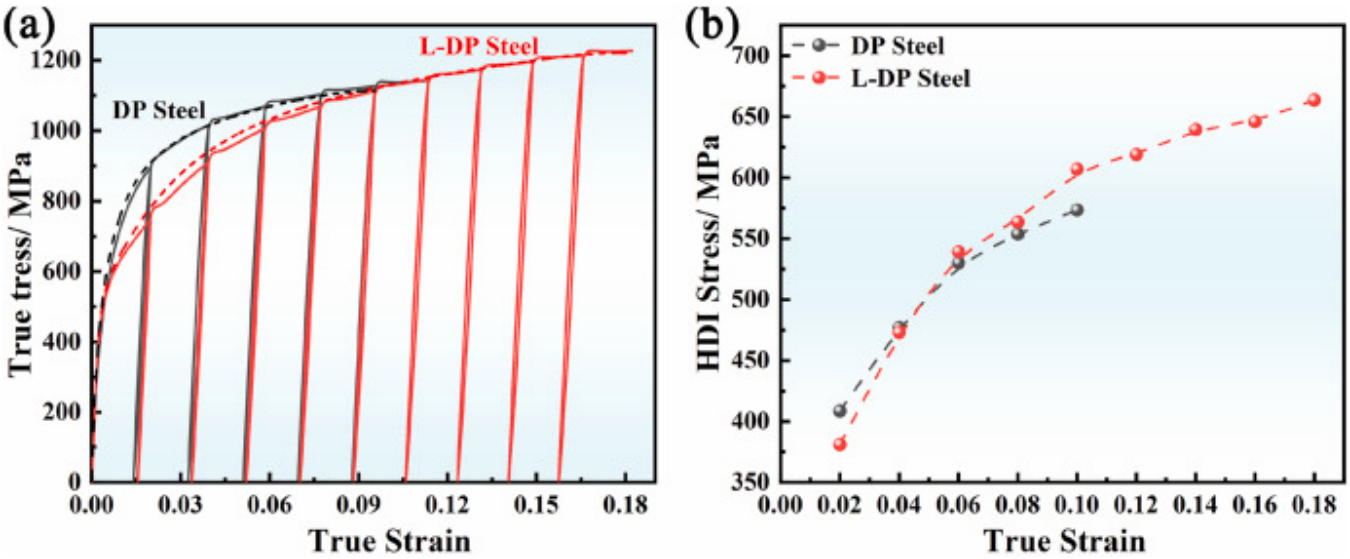

1. Download: Download high-res image (543KB)
2. Download: Download full-size image

Fig. 11. Cyclic loading–unloading–reloading (LUR) tensile tests
(a) LUR true stress-strain curve (solid line) and uniaxial tensile true stress-strain curve(dotted line) in the DP and L-DP steels. (b) Variation of measured back stress versus true strain in the two steels.

It can be observed from Fig. 11a that the LUR curves are almost consistent with the uniaxial tensile curves, indicating the outstanding repeatability of the mechanical properties of the two steels and the reliability of the experimental data. A detailed calculation reveals that the HDI stress in both the DP and L-DP steels increases with the increase of strain, as shown in Fig. 11b. In the early stage of deformation ($\varepsilon \leq 0.04$), the DP steel exhibits higher HDI stress than the L-DP steel. However, after this stage ($\varepsilon > 0.04$), the HDI stress of L-DP steel exceeds that of DP steel and remains ahead. The dual-phase microstructure composed of block martensite and polygonal ferrite in DP steel belongs to a type of heterogeneous microstructure [60]. Due to the mechanical incompatibility in the dual-phase microstructure during the deformation process, the occurrence of strain gradients leads to the accumulation of geometrically necessary dislocations at the phase interface, ultimately inducing back stress (HDI hardening) [57]. Generally, the high heterogeneity of heterogeneous microstructure leads to high strain gradients, resulting in high back stress. Therefore, high back stress is generated in the early stage of deformation in the DP steel. However, as plastic deformation continues, polygonal ferrite is difficult to be effectively constrained by block martensite, which tends to cause local stress concentration at the phase interface or inside the ferrite. This promotes the formation of micropores or ferrite yielding, ultimately slowing down the trend of increasing back stress. As the tensile strain further increases, severe local stress concentration leads to the formation of numerous micropores and martensitic cracks, thereby promoting the fracture of DP steel.

In contrast, since the hardness difference between lamellar martensite and ferrite in the L-DP steel is less than that in the DP steel, the back stress in the L-DP steel is less than

that in the DP steel during the initial deformation stage. However, the relatively low hardness difference and special lamellar microstructure make the L-DP steel have appreciable deformation coordination during subsequent plastic deformation without causing excessive stress concentration. As the deformation progresses into the stable plastic deformation stage, the back stress of the L-DP steel continues to steadily increase due to the typical heterogeneous lamellar microstructure ensuring the continuous mutual restraint of lamellar martensite to lamellar ferrite. Therefore, under the combined action of considerable synergistic deformation and continuous HDI hardening of lamellar martensite and lamellar ferrite, the L-DP steel obtains continuous work hardening, thus achieving high strength and high plasticity synergy.

4.3. Deformation mechanisms of different microstructures

To further elucidate the plastic deformation mechanism inherent in the L-DP steel, we have drawn a schematic diagram of the entire plastic deformation process based on the above-observed characteristics and combined it with in-situ SEM evidence, as shown in Fig. 12. A schematic of the plastic deformation of DP steel is used to aid in the illustration. In Fig. 12a, a representative region from the DP steel is selected as the analysis object. As depicted in Fig. 12a1, the phase interface stress starts accumulating at the initial stage of deformation. As the deformation continues, the stress on the block martensite and polygonal ferrite regions significantly increases, eventually reaching the yield stress, as illustrated in Fig. 12a2. After yielding DP steel, the significant difference in hardness and structural characteristics between block martensite and polygonal ferrite leads to poor deformation coordination, resulting in pronounced stress concentration both at the phase interface and softer ferrite. The stress concentration at the phase interface and inside the ferrite is released only through the formation of voids, as shown in Fig. 12a3. With the further increase of tensile strain, the block martensite lacks the ability for continuous work hardening and thus undergoes brittle cracking (Fig. 12a4) under the rapid accumulation of high stress [61]. This phenomenon ultimately leads to premature cracking in the DP steel during deformation, with an abundance of voids and cracks evident at the fracture (Fig. 7, Fig. 8a). In contrast, the L-DP steel consists of alternately arranged lamellar martensite and lamellar ferrite. Similarly, a representative region from the L-DP steel is selected as the analysis object, as shown in Fig. 12b and c. As the tensile strain increases, most of the lamellar martensite and lamellar ferrite gradually changes from the initial random distribution to parallel with the tensile direction (Fig. 12b1 and Fig. 12d). The frequent alternation of soft and hard lamellae and the smaller hardness difference are less likely to cause significant stress concentrations at the ferrite or martensite/ferrite phase interface. With further increase in strain, the work hardening of lamellar ferrite is obvious, which causes the plastic deformation of lamellar martensite and lamellar ferrite together. The lamellar martensite and ferrite with larger angles relative to the tensile direction undergo co-deformation by bending together (Fig. 12b2-12b4 and Fig. 12d–i). Conversely, the lamellar martensite and ferrite with small angles relative to the tensile direction are significantly stretched and thinned (Fig. 12b3 and Fig. 12e). Therefore, the severe plastic deformation of the L-DP steel verifies the excellent coordination deformation ability of lamellar martensite and lamellar ferrite. As the tensile strain continues to increase, a small number of microcracks and voids are generated to alleviate stress concentration (Fig. 12b4 and Fig. 12f). Since most of the

lamellae at this point are already approximately parallel to the tensile direction (Fig. 12g and h), the interconnection of microcracks is hindered, thus ensuring that the L-DP steel can continue to deform. Therefore, the remarkable ductility of the L-DP steel, while maintaining high strength, is attributed to the thoughtful design of the lamellar microstructure with excellent coordinated deformation ability and hetero-deformation-induced strengthening ability.

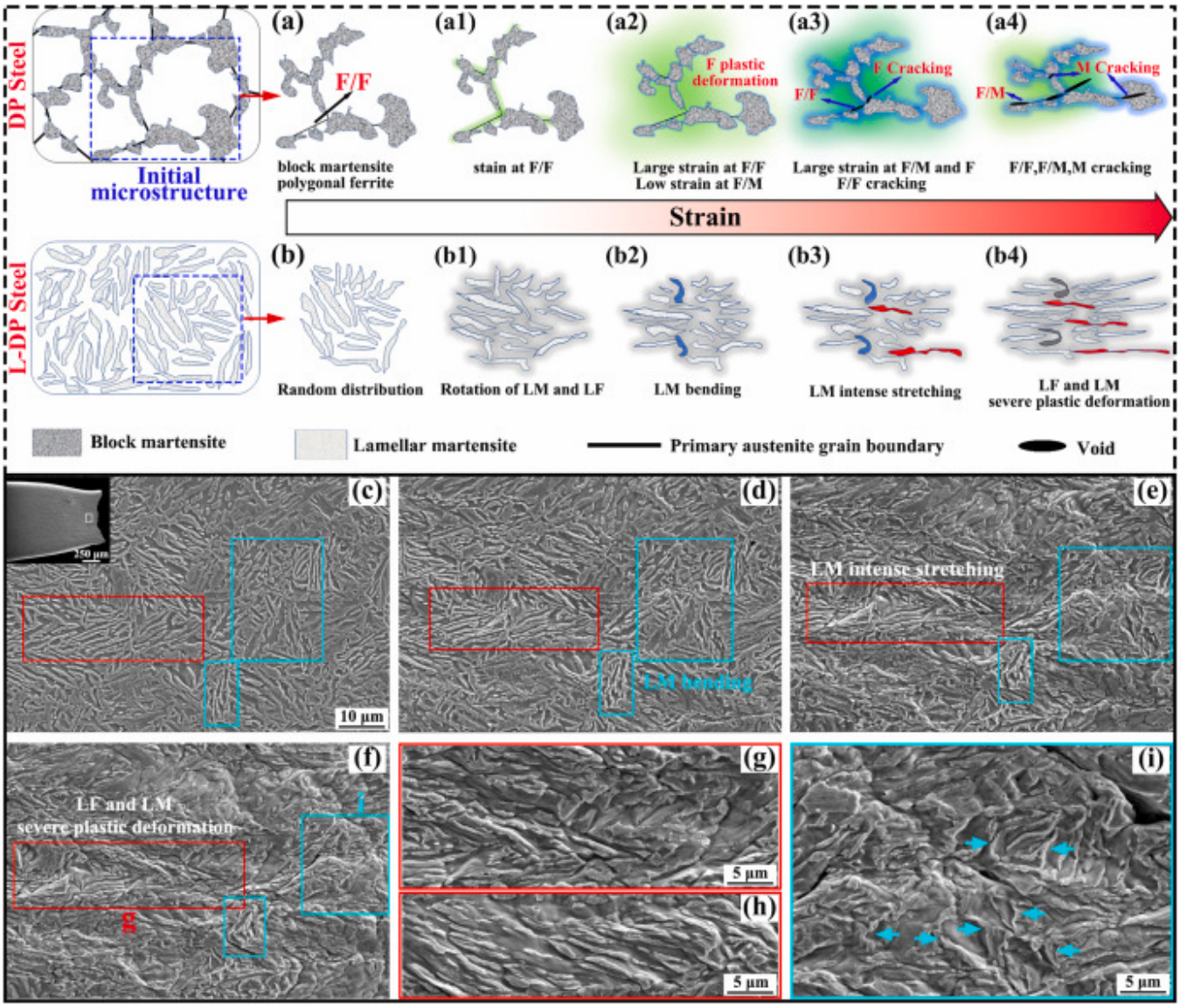

1. Download: Download high-res image (2MB)
2. Download: Download full-size image

Fig. 12. The schematic diagram of the deformation mechanism of DP steel (a-a4) and L-DP steel (b-b4). LM and LF indicate lamellar martensite and lamellar ferrite, respectively. (c–i) In-situ SEM images of the L-DP steel under different tensile strains: (c) 0 %, (d) 6.9 %, (c) 17.2 %, (f) Fracture. The red and light green boxes indicate the stretching and bending processes of the lamellar microstructure, respectively. (g) A magnified SEM image of the marked area in f. (h) A magnified SEM image of the fracture

morphology (outside the field of view in f). (i) A magnified SEM image of the marked area in f. The arrows indicate the bent lamellar martensite. More details of the microstructure evolution are shown in Fig. S6. (For interpretation of the references to colour in this figure legend, the reader is referred to the Web version of this article.)

5. Conclusions

1) In this study, dual-phase steels with alternating lamellar ferrite and lamellar martensite microstructures are fabricated using a cyclic intercritical quenching process based on non-equilibrium phase transformation. The lamellar martensite and ferrite exhibit heterogeneity at the micro level and are randomly and uniformly distributed at the macro level. The cyclic intercritical quenching process refines the lamellar microstructure and reduces the elemental concentration difference between ferrite and martensite, thereby decreasing the distortion and hardness differences between the two phases.
2) The novel L-DP steel exhibits remarkable mechanical properties, featuring a UTS of approximately 1034 MPa, UE of about 17.3 %, and TE of approximately 25.3 %. In contrast, the conventional DP steel with the same composition and phase volume fraction shows lower UTS (~1002 MPa) and reduced ductility (UE ~9.1 %, TE ~16.3 %). The L-DP steel displays an outstanding 90 % increase in UE without any compromise in UTS. Although the individual values of UTS and UE are not the highest among GPa-grade AHSSs, the optimal combination of UTS and UE makes the L-DP steel stand out.
3) The simultaneous improvement of ultimate tensile strength and ductility of L-DP steel is attributed to the thoughtful design of the lamellar microstructure with the appropriate hardness difference. The excellent plastic deformation ability of lamellar martensite and the outstanding deformation coordination of the lamellar microstructure in the L-DP steel allow for persistent work hardening without premature cracking during plastic deformation. Additionally, the hetero-deformation-induced hardening generated by the mutually constrained lamellar martensite and lamellar ferrite during plastic deformation provides additional work hardening.

CRediT authorship contribution statement

Gang Niu: Conceptualization, Investigation, Methodology, Writing – original draft, Writing – review & editing. **Chao Ding:** Formal analysis, Investigation, Methodology, Validation, Writing – review & editing. **Zhiying Liu:** Formal analysis, Methodology, Validation. **Xiaohang Jia:** Formal analysis, Validation. **Haoxiu Chen:** Formal analysis, Methodology. **Na Gong:** Conceptualization, Formal analysis, Writing – review & editing. **Yong Wang:** Formal analysis, Validation. **Dennis TAN. Cheng Cheh:** Writing – review & editing. **R.D.K. Misra:** Writing – review & editing. **Huibin Wu:** Conceptualization, Project administration, Writing – review & editing.

Declaration of competing interest

The authors declare that they have no known competing financial interests or personal relationships that could have appeared to influence the work reported in this paper.

Acknowledgment

G. Niu, C. Ding, N. Gong, and H.B. Wu appreciate the support from the National Natural Science Foundation of China (Grant No. 52304389). G. Niu appreciates the support from the China Postdoctoral Science Foundation (2022M720402). G. Niu and H.B. Wu appreciate the support from the Fundamental Research Funds for the Central Universities (FRF-BD-23-01). N. Gong and D. Tan appreciate the support from the Structural Metal Alloy Program, Singapore (SMAP), Grant No. A18B1b0061, and Manufacturing of Multi-Material Net-Shape Parts with Heterogeneous Properties (MMNH), Singapore, Grant No. M22K5a0045 in A*STAR. N. Gong thanks her former advisor, Professor R.D.K. Misra at UTEP for careful reading and review of the manuscript.

Appendix A. Supplementary data

The following is the Supplementary data to this article.

Download: Download Word document (10MB)

Multimedia component 1.

Data availability

Data will be made available on request.

References

[1]

S. Basu, B.N. Jaya, A. Patra, S. Ganguly, M. Dutta, A. Hohenwarter, I. Sa majdar

The role of phase hardness differential on the non-uniform elongation of a ferrite-martensite dual phase steel

Metall. Mater. Trans. A, 52 (2021), pp. 4018-4032

CrossrefView in ScopusGoogle Scholar
[2]

R.D.K. Misra

Strong and ductile texture-free ultrafine-grained magnesium alloy via three-axial forging

Mater. Lett., 331 (2023)

Article 133443

Google Scholar
[3]

G. Niu, H.S. Zurob, R.D.K. Misra, Q. Tang, Z. Zhang, M.-
T. Nguyen, L. Wang, H. Wu, Y. Zou

Superior fracture toughness in a high-strength austenitic steel with heterogeneous lamellar microstructure

Acta Mater., 226 (2022)

Article 117642

Google Scholar
[4]

H. Ning, X. Li, L. Meng, A. Jiang, B. Ya, S. Ji, W. Zhang, J. Du, X. Zhang

Effect of Ni and Mo on microstructure and mechanical properties of grey cast iron

Mater. Technol., 38 (2023)

Article 2172991

Google Scholar
[5]

M.R. Weaver, A.J. Maldonado, J.L. Banuelos, R.D.K. Misra

On precipitation hardening behaviour in a triaxial forged Mg-2Zn-2Gd alloy and relationship to mechanical properties

Mater. Technol., 38 (2023)

Article 2215038

Google Scholar
[6]

R.D.K. Misra, V.S.A. Challa, V.S.Y. Injeti

Phase reversion-induced nanostructured austenitic alloys: an overview

Mater. Technol., 37 (2022), pp. 437-449

CrossrefView in ScopusGoogle Scholar
[7]

G. Niu, H.S. Zurob, R. Misra, H. Wu, Y. Zou

Strength-ductility synergy in a 1.4 GPa austenitic steel with a heterogeneous lamellar microstructure

J. Mater. Sci. Technol., 106 (2022), pp. 133-138

View PDFView articleView in ScopusGoogle Scholar
[8]

Q. Jia, L. Chen, X. Chen, H. Choi, Z. Xing, S. Lee, H. Kim, H. Wang, H. H uang, M. Jin

Enhancing strength–ductility synergy in medium Mn steel with hetero-structured austenite developed by two-stage cyclic thermomechanical treatment and flash annealing

Scr. Mater., 226 (2023)

Article 115196

Google Scholar
[9]

Q. Jia, L. Chen, Z. Xing, H. Wang, M. Jin, X. Chen, H. Choi, H.N. Han

Tailoring hetero-grained austenite via a cyclic thermomechanical process for achieving ultrahigh strength-ductility in medium-Mn steel

Scr. Mater., 217 (2022)

Article 114767

Google Scholar
[10]

T.W.J. Kwok, D. Dye

A review of the processing, microstructure and property relationships in medium Mn steels

Int. Mater. Rev. (2023), pp. 1-37

CrossrefGoogle Scholar
[11]

B. Sun, A. Kwiatkowski da Silva, Y. Wu, Y. Ma, H. Chen, C. Scott, D. Ponge, D. Raabe

Physical metallurgy of medium-Mn advanced high-strength steels

Int. Mater. Rev. (2023), pp. 1-39

Google Scholar
[12]

V. Atreya, C. Bos, M.J. Santofimia

Understanding ferrite deformation caused by austenite to martensite transformation in dual phase steels

Scr. Mater., 202 (2021)

Article 114032

Google Scholar
[13]

R. Song, D. Ponge, D. Raabe, J.G. Speer, D.K. Matlock

Overview of processing, microstructure and mechanical properties of ultrafine grained bcc steels

Mater. Sci. Eng.A, 441 (2006), pp. 1-17

View PDFView articleView in ScopusGoogle Scholar
[14]

K. Ismail, A. Perlade, P.J. Jacques, T. Pardoen, L. Brassart

Impact of second phase morphology and orientation on the plastic behavior of dual-phase steels

Int. J. Plasticity., 118 (2019), pp. 130-146

View PDFView articleView in ScopusGoogle Scholar
[15]

M. Alibeyki, H. Mirzadeh, M. Najafi

Fine-grained dual phase steel via intercritical annealing of cold-rolled martensite

Vacuum, 155 (2018), pp. 147-152

View PDFView articleView in ScopusGoogle Scholar
[16]

M. Soleimani, H. Mirzadeh

Enhanced mechanical properties of dual phase steel via cross rolling and intercritical annealing

Mater. Sci. Eng.A, 804 (2021)

Article 140778

Google Scholar
[17]

N. Tsuji, Y. Ito, Y. Saito, Y. Minamino

Strength and ductility of ultrafine grained aluminum and iron produced by ARB and annealing

Scr. Mater., 47 (2002), pp. 893-899

View PDFView articleView in ScopusGoogle Scholar
[18]

A.A. Sayed, S. Kheirandish

Affect of the tempering temperature on the microstructure and mechanical properties of dual phase steels

Mater. Sci. Eng.A, 532 (2012), pp. 21-25

View PDFView articleView in ScopusGoogle Scholar
[19]

M.D. Taylor, E. De Moor, J.G. Speer, D.K. Matlock

Effects of constituent hardness on formability of dual phase steels

Steel Res. Int., 92 (2021), Article 2100281

View in ScopusGoogle Scholar
[20]

Q. Han, A. Asgari, P.D. Hodgson, N. Stanford

Strain partitioning in dual-phase steels containing tempered martensite

Mater. Sci. Eng.A, 611 (2014), pp. 90-99

View PDFView articleView in ScopusGoogle Scholar
[21]

S. Gündüz

Effect of chemical composition, martensite volume fraction and tempering on tensile behaviour of dual phase steels

Mater. Lett., 63 (2009), pp. 2381-2383

View PDFView articleView in ScopusGoogle Scholar
[22]

C.-n. Li, G. Yuan, F.-q. Ji, D.-s. Ren, G.-d. Wang

Effects of auto-tempering on microstructure and mechanical properties in hot rolled plain C-Mn dual phase steels

Mater. Sci. Eng.A, 665 (2016), pp. 98-107

View PDFView articleView in ScopusGoogle Scholar
[23]

E. Chandiran, N. Kamikawa, Y. Sato, G. Miyamoto, T. Furuhara

Improvement of strength–ductility balance by the simultaneous increase in ferrite and martensite strength in dual-phase steels

Metall. Mater. Trans. A, 52 (2021), pp. 5394-5408

CrossrefView in ScopusGoogle Scholar
[24]

N. Kamikawa, M. Hirohashi, Y. Sato, E. Chandiran, G. Miyamoto, T. Furuhara

Tensile behavior of ferrite-martensite dual phase steels with nano-precipitation of vanadium carbides

ISIJ Int., 55 (2015), pp. 1781-1790

View in ScopusGoogle Scholar
[25]

F. Yaghoobi, R. Jamaati, H. Jamshidi Aval

Simultaneous enhancement of strength and ductility in ferrite-martensite steel via increasing the martensite fraction

Mater. Chem. Phys., 259 (2021)

Article 124204

Google Scholar
[26]

A. Ebrahimian, S.S. Ghasemi Banadkouki

Mutual mechanical effects of ferrite and martensite in a low alloy ferrite-martensite dual phase steel

J. Alloys Compd., 708 (2017), pp. 43-54

View PDFView articleView in ScopusGoogle Scholar
[27]

S.-P. Tsai, C.-H. Jen, H.-W. Yen, C.-Y. Chen, M.-C. Tsai, C.-Y. Huang, Y.-T. Wang, J.-R. Yang

Effects of interphase TiC precipitates on tensile properties and dislocation structures in a dual phase steel

Mater. Char., 123 (2017), pp. 153-158

View PDFView articleView in ScopusGoogle Scholar
[28]

A.P. Pierman, O. Bouaziz, T. Pardoen, P.J. Jacques, L. Brassart

The influence of microstructure and composition on the plastic behaviour of dual-phase steels

Acta Mater., 73 (2014), pp. 298-311

View PDFView articleView in ScopusGoogle Scholar
[29]

D. Das, P.P. Chattopadhyay

Influence of martensite morphology on the work-hardening behavior of high strength ferrite–martensite dual-phase steel

J. Mater. Sci., 44 (2009), pp. 2957-2965

CrossrefView in ScopusGoogle Scholar
[30]

X. Wu, M. Yang, F. Yuan, G. Wu, Y. Wei, X. Huang, Y. Zhu

Heterogeneous lamella structure unites ultrafine-grain strength with coarse-grain ductility

Proc Natl Acad Sci U S A, 112 (2015), pp. 14501-14505

CrossrefView in ScopusGoogle Scholar
[31]

R. Yuan, I.J. Beyerlein, C. Zhou

Homogenization of plastic deformation in heterogeneous lamella structures

Mater. Res. Lett., 5 (2017), pp. 251-257

CrossrefView in ScopusGoogle Scholar
[32]

J. Zhang, Y. Xu, Y. Wang, S. Wang

Achieving heterogeneous TWIP/TRIP steel with 1GPa strength and 72% ductility by introducing austenite + martensite lamella structure

Mater. Char., 197 (2023)

Article 112709

Google Scholar
[33]

B. Gao, R. Hu, Z. Pan, X. Chen, Y. Liu, L. Xiao, Y. Cao, Y. Li, Q. Lai, H. Z hou

Strengthening and ductilization of laminate dual-phase steels with high martensite content

J. Mater. Sci. Technol., 65 (2021), pp. 29-37

View PDFView articleView in ScopusGoogle Scholar
[34]

J.X. Huang, Y. Liu, T. Xu, X.F. Chen, Q.Q. Lai, L.R. Xiao, Z.Y. Pan, B. Ga o, H. Zhou, Y.T. Zhu

Dual-phase hetero-structured strategy to improve ductility of a low carbon martensitic steel

Mater. Sci. Eng.A, 834 (2022)

Article 142584

Google Scholar
[35]

J. Sun, T. Jiang, Y. Wang, S. Guo, Y. Liu

Ultrafine grained dual-phase martensite/ferrite steel strengthened and toughened by lamella structure

Mater. Sci. Eng.A, 734 (2018), pp. 311-317

View PDFView articleView in ScopusGoogle Scholar
[36]

M.D. Zhang, J. Hu, W.Q. Cao, H. Dong

Microstructure and mechanical properties of high strength and high toughness micro-laminated dual phase steels

Mater. Sci. Eng.A, 618 (2014), pp. 168-175

View PDFView articleView in ScopusGoogle Scholar
[37]

M.B. Sk, I. Alam, D. Chakrabarti

The role of fibrous morphology on the Charpy impact properties of low carbon ferrite-bainite dual phase steel

Mater. Sci. Eng.A, 716 (2018), pp. 208-219

View PDFView articleView in ScopusGoogle Scholar
[38]

E.I. Hernandez-Duran, V. Bliznuk, T. Ros-Yanez, R. Iquilio-Abarzua, F.M. Castro-Cerda, R.H. Petrov

Improvement of the strength-ductility balance in ultrafast heated steels by combining high-temperature annealing and quenching and partitioning process

Mater. Sci. Eng.A, 827 (2021)

Article 142045

Google Scholar
[39]

N. Xu, L. Wang, J. Hu, H. Liu, S. Yu, W. Xu

Batch annealing enhances the yield strength of a high quenching temperature Q&P steel through accelerated bainitic transformation

Mater. Sci. Eng.A, 855 (2022), Article 143888

View PDFView articleView in ScopusGoogle Scholar
[40]

F. Zhang, A. Ruimi, P.C. Wo, D.P. Field

Morphology and distribution of martensite in dual phase (DP980) steel and its relation to the multiscale mechanical behavior

Mater. Sci. Eng.A, 659 (2016), pp. 93-103

View PDFView articleView in ScopusGoogle Scholar
[41]

A. Tang, H. Liu, R. Chen, G. Liu, Q. Lai, Y. Zhong, L. Wang, J. Wang, Q. L u, Y. Shen

Mesoscopic origin of damage nucleation in dual-phase steels

Int. J. Plasticity, 137 (2021)

Article 102920

Google Scholar
[42]

C. Zhang, C. Liu, H. Guo, S. Sun, H. Chen, Y. Liu, R. Ding

Chemical heterogeneity enables austenite stabilization in a Si-/Al-free Fe-0.2C-2Mn steel

Scr. Mater., 218 (2022)

Article 114822

Google Scholar
[43]

H. Ashrafi, M. Shamanian, R. Emadi, N. Saeidi

A novel and simple technique for development of dual phase steels with excellent ductility

Mater. Sci. Eng.A, 680 (2017), pp. 197-202

View PDFView articleView in ScopusGoogle Scholar
[44]

A. Kundu, D.P. Field

Influence of plastic deformation heterogeneity on development of geometrically necessary dislocation density in dual phase steel

Mater. Sci. Eng.A, 667 (2016), pp. 435-443

View PDFView articleView in ScopusGoogle Scholar
[45]

C. Ding, J. Liu, B. Ning, M. Huang, H. Wu

Enhanced strength-plasticity matching of lamellar 1 GPa-grade dual-phase steels via cyclic intercritical quenching

J. Mater. Res. Technol., 22 (2023), pp. 3115-3131

View PDFView articleView in ScopusGoogle Scholar
[46]

X. Zhang, G. Miyamoto, T. Kaneshita, Y. Yoshida, Y. Toji, T. Furuhara

Growth mode of austenite during reversion from martensite in Fe-2Mn-1.5Si-0.3C alloy: a transition in kinetics and morphology

Acta Mater., 154 (2018), pp. 1-13

View PDFView articleGoogle Scholar
[47]

R. Ding, Z. Dai, M. Huang, Z. Yang, C. Zhang, H. Chen

Effect of pre-existed austenite on austenite reversion and mechanical behavior of an Fe-0.2C-8Mn-2Al medium Mn steel

Acta Mater., 147 (2018), pp. 59-69

View PDFView articleView in ScopusGoogle Scholar
[48]

A. Kalhor, A. Karimi Taheri, H. Mirzadeh, V. Uthaisangsuk

Processing, microstructure adjustments, and mechanical properties of dual phase steels: a review

Mater. Sci. Technol., 37 (2021), pp. 561-591

CrossrefView in ScopusGoogle Scholar
[49]

L. Qian, K. Li, F. Huang, D. Li, T. Wang, J. Meng, F. Zhang

Enhancing both strength and ductility of low-alloy transformation-induced plasticity steel via hierarchical lamellar structure

Scr. Mater., 183 (2020), pp. 96-101

View PDFView articleView in ScopusGoogle Scholar

[50]

Q.L. Jiang, Y.J. Li, J. Wang, L. Zhang

Effects of Mn and Ti on microstructure and inclusions in weld metal of high strength low alloy steel

Mater. Sci. Technol., 27 (2011), pp. 1385-1390

View in ScopusGoogle Scholar
[51]

Q. Lu, W. Xu, S.v.d. Zwaag

Designing new corrosion resistant ferritic heat resistant steel based on optimal solid solution strengthening and minimisation of undesirable microstructural components

Comp. Mater. Sci., 84 (2014), pp. 198-205

View PDFView articleView in ScopusGoogle Scholar
[52]

M. Calcagnotto, D. Ponge, E. Demir, D. Raabe

Orientation gradients and geometrically necessary dislocations in ultrafine grained dual-phase steels studied by 2D and 3D EBSD

Mater. Sci. Eng.A, 527 (2010), pp. 2738-2746

View PDFView articleView in ScopusGoogle Scholar
[53]

S. Sodjit, V. Uthaisangsuk

Microstructure based prediction of strain hardening behavior of dual phase steels

Mater. Des., 41 (2012), pp. 370-379

View PDFView articleView in ScopusGoogle Scholar
[54]

M. Mazinani, W.J. Poole

Effect of martensite plasticity on the deformation behavior of a low-carbon dual-phase steel

Metall. Mater. Trans. A, 38 (2007), pp. 328-339

CrossrefView in ScopusGoogle Scholar
[55]

E. Chandiran, Y. Sato, N. Kamikawa, G. Miyamoto, T. Furuhara

Effect of ferrite/martensite phase size on tensile behavior of dual-phase steels with nano-precipitation of vanadium carbides

Metall. Mater. Trans. A, 50 (2019), pp. 4111-4126

CrossrefView in ScopusGoogle Scholar
[56]

N.K. Patel, M.G. Walunj, B. Ravi Kumar

Importance of martensite spatial distribution at large volume fractions in imparting ductility in high-strength dual-phase steel

J. Mater. Eng. Perform., 28 (2019), pp. 1391-1401

CrossrefView in ScopusGoogle Scholar
[57]

Y. Zhu, X. Wu

Perspective on hetero-deformation induced (HDI) hardening and back stress

Mater. Res. Lett., 7 (2019), pp. 393-398

CrossrefGoogle Scholar
[58]

Y. Zhu, K. Ameyama, P.M. Anderson, I.J. Beyerlein, H. Gao, H.S. Kim, E. Lavernia, S. Mathaudhu, H. Mughrabi, R.O. Ritchie, N. Tsuji, X. Zhang, X. Wu

Heterostructured materials: superior properties from hetero-zone interaction

Mater. Res. Lett., 9 (2021), pp. 1-31

Google Scholar
[59]

M. Yang, Y. Pan, F. Yuan, Y. Zhu, X. Wu

Back stress strengthening and strain hardening in gradient structure

Mater. Res. Lett., 4 (2016), pp. 145-151

CrossrefView in ScopusGoogle Scholar
[60]

Y. Zhu, X. Wu

Heterostructured materials

Prog. Mater. Sci., 131 (2023), Article 101019

View PDFView articleView in ScopusGoogle Scholar
[61]

H.S. Oh, K. Biggs, O. Güvenç, H. Ghassemi-Armaki, N. Pottore, C.C. Tasan

In-situ investigation of strain partitioning and microstructural strain path development up to and beyond necking

Acta Mater., 215 (2021)

Article 117023

Google Scholar